Proceedings of ASME Turbo Expo 2022
Turbomachinery Technical Conference and Exposition
GT2022
June 13-17, 2022, Rotterdam, The Netherlands

GT2022-80865

QUASI-TWO-DIMENSIONAL NUMERICAL MODEL FOR SHOCK WAVE REFORMERS

Ghislain Madiot
Simon Fraser University
Vancouver, Canada

S. V. Mahmoodi-Jezeh
Simon Fraser University
Vancouver, Canada

Stefan Tüchler
University of Bath,
Bath, United Kingdom

Mark Davidson
New Wave Hydrogen, Inc.,
Gainesville, USA

Pejman Akbari
California State Polytechnic University
Pomona, USA

Colin D. Copeland
Simon Fraser University
Vancouver, Canada

ABSTRACT

The article details a numerical investigation of methane pyrolysis inside a shock wave reformer using a quasi-2-dimensional (Q2D) Reynolds-Averaged Navier–Stokes (RANS) CFD model. This work is in support of the New Wave Hydrogen, Inc. (NWH_2) proprietary technology development. To take account of the characteristics of the flow in the presence of shock waves, a simplified approach is proposed that captures the gas dynamics during partial opening with a lower computational cost suitable for the wave reformer design. The model is based on the three-dimensional, compressible, and unsteady Navier-Stokes equation coupled with $k-\omega$ - SST turbulence closure. Boundary conditions are implemented through a cell-centered approach with fictitious cells outside of the domain boundaries. The numerical results are compared with solutions from a quasi-one-dimensional (Q1D) unsteady model reported in literature. The simulations show a good agreement between the two different modelling approaches in terms of spatial distribution of the pressure gradient for one complete cycle. It is observed from the Q2D results that the entrance for each passage, especially upon opening of the high-pressure driver gas port, is a location of particular interest in the formation of the shock. The resulting acute pressure gradients induce loss inside the channel, decreasing the maximum temperature during a complete wave cycle by 15%, and consequently, reducing the methane pyrolysis process.

Keywords: wave reformer, wave rotor, methane pyrolysis, shock heating, wave chemical reactor, hydrogen.

NOMENCLATURE

3D	three-dimensional
CFD	computational fluid dynamics
GHG	greenhouse gases
HP	high pressure
LHS	left hand side
LP	low pressure
NWH_2	New Wave Hydrogen Inc
Q1D	quasi-one-dimensional
Q2D	quasi-two-dimensional
RANS	Reynolds-Averaged Navier–Stokes
RHS	right hand side
SMR	steam methane reforming
SST	shear stress transport

1. INTRODUCTION

To ensure access to sustainable, affordable, reliable, and clean energy for all, the energy sector must be transformed. Hydrogen offers an excellent potential to replace much of the fossil fuel use. At present, the main methods of hydrogen production typically release a non-negligeable volume of greenhouse gases (GHG) either directly via fossil fuel transformation or indirectly through power generation. In addition, hydrogen production commonly requires a significant consumption of fresh water. Indeed, steam methane reforming (SMR) which is the most common hydrogen production process, involves a high-temperature process in which steam reacts with a hydrocarbon fuel to produce hydrogen [1]. Alternatively, electrolysis splits hydrogen from water using electricity [2]. In contrast, Wave Reforming, a patented method by New Wave Hydrogen Inc. (NWH2), introduces an innovative concept for hydrogen conversion [3] using shock wave heating in a wave rotor device. The concept is based on a well-known process, methane pyrolysis, and an existing

technology, a wave rotor, to produce hydrogen and easily separable solid carbon. The reformer utilizes the high pressure present in the natural gas supply infrastructure and thus, requires little change to existing energy or water supplies.

In comparison with conventional turbomachines that exchange fluid energy by shaft work, in a wave rotor, the energy exchange between two fluids is conducted by pressure/expansion wave propagation to exchange energy between high and low enthalpy gas streams. Wave rotors are known to be unique in many ways, including but not limited to, the ease of scaling in size and the potential for maintaining a wall material temperature lower than the peak gas temperature inside the channel. The fundamental principle of the rotor wave is similar to a shock tube, except that a wave rotor has rotating parts that cause the waves to propagate continuously and an inflow and outflow of gas that forms a repeating cycle. One of the main features of the system is that no mechanical components such as piston nor impeller are required to compress the gas. To achieve this, a wave rotor consists of an array of channels arranged in parallel around a rotating cylinder drum and two stationary end plates with ports on them. The concept becomes clearer when the circumferential surface is developed and plotted on a two-dimensional plane - θ-L (θ can also be considered as the time). This allows a viewer to follow a channel as it rotates and passes the port openings in the process. In the illustrated example in Fig. 1(a), a schematic configuration of four-port throughflow (fluid flow only in one direction) rotor is shown. A two-dimensional plane or wave diagram is presented by Fig. 1(b). On the left hand side, the wave rotor alternatively permits an inflow of low-pressure and high-pressure gas into a rotating channel. The channel is first filled by the low-pressure gas (LPF2). The high-pressure gas (HPF1) triggers a shock wave propagation represented by a solid black line. This shock wave generates high pressure and thermal peaks in the driven gas. Finally, the gases flow out of the ports with some inherent mixing that depend on the cycle.

This technology has been used on a large spectrum of applications from supercharging devices [4] to refrigeration cycles [5] and cycle topping for gas turbines [6], where it was used to boost the turbine inlet pressure. A comprehensive review of the range of activities is provided in a review by Akbari et. al [7]. In the early 1990s, Paxon [8], developed a quasi-one-dimensional CFD method based on the Euler equations. The model could predict the major loss mechanisms including finite passage opening time and fluid friction. This model was validated in a test-rig for a four-port through -flow design. Shortly after, Welch [9] presented a two dimensional Navier-Stokes based solver for wave rotor that can estimated work transferred to or from the fluid for partial opening with blade profile.

Recently, Chan et al. [10] proposed a general method to design wave rotors. The study highlights the importance of the experiment as a standard procedure and suggested to use the CFD design tool to primarily determine the key parameter such as the basic geometry, the rotation speed, the internal cyclic flow patterns, and the performance of the wave rotor.

Around the same period, Tüchler and Copeland [11–13] dedicated some effort to develop numerical modeling for a wave rotor. One of the studies focused on two-dimensional shapes optimization of wave rotor channel using genetic algorithms to improve the shaft power. To minimize the computational cost required, a Q2D numerical model was introduced. The numerical trends from the optimised design are compared with a three-dimensional-model and approved using experimental data [13]. Additional works were conducted on the numerical tools including description of the numerical approach, investigation on loss modeling, and boundary condition implementations.

More recently, NWH_2 [3] introduces a new proprietary method of methane pyrolysis in a rotary chemical reactor using wave rotor technology. The wave reformer makes use of the sharp temperature peak behind the moving shock to initiate a

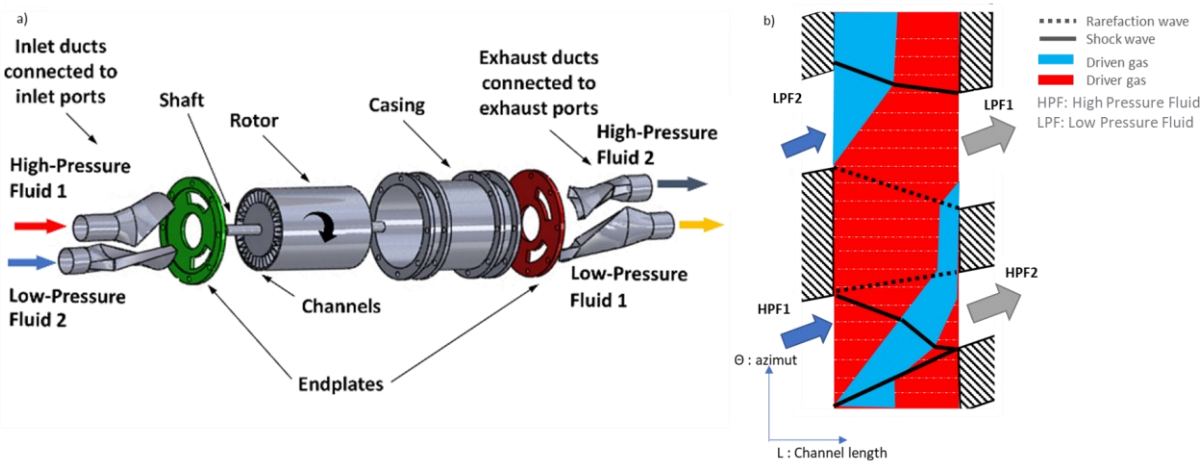

FIGURE 1: REPRESENTATION OF FOUR-PORT WAVE ROTOR, (A) SCHEMATIC CONFIGURATION OF A TYPICAL WAVE ROTOR (B) VIEW OF A DEVELOPED SURFACE OF THE WAVE PATTERN.

thermal decomposition reaction in gaseous constituents within its channels. Since the conversion and kinetics of the reaction are the main objectives, the design aims to maximize the peak temperature and residence time of a reactant gas.

The first results based on the customized version of the Tüchler-Copeland Q1D CFD code [3] showed sufficient peak temperatures and residence times to achieve efficient H_2 production. Subsequently, Mahmoodi-Jezeh et al. [14], in a companion to this paper, have aimed to validate the chemical model used for predicting the thermal decomposition of methane into hydrogen and carbon within a four-port reverse flow wave rotor single channel.

Despite the above-mentioned contributions, the research in the past does not cover the pyrolysis of hydrocarbons in wave rotors since simply, this is a new concept. Thus, CFD methods for the parametric analysis of wave rotor chemical reformation is a gap to be addressed in this work. This paper will particularly focus on multi-channel wave rotor signs, thus being distinct from the single shock tube design in the companion paper [14]. In addition, this paper will aim to propose a CFD simulation methodology that will enable the design optimization of a multichannel wave rotor reformer. The proposed methodology aims at reducing the computational effort while maintaining good agreement between the different modelling approaches in terms of spatial distribution of the pressure gradient for one complete cycle.

2. METHOD DESCRIPTION

2.1 Geometry cases

Various wave cycles can be designed in multi-channel setup. Different wave cycles are characterized by the number of inlet and exit ports, residence time, and peak temperature and wave timing. The well-established technology in literature is a four-port wave rotor which has been the subject of numerous studies in the past. The present paper will feature completely new cycles that are tailored to maximize pyrolysis by maximizing temperature and residence time.

Figure 2 introduces an unwrapped display of different wave reformer cycles with a channel moving upward. In the figure, HP and LP refer to high-pressure and low-pressure gases, respectively. The primary and secondary shocks are represented with the black solid lines, the expansion waves with dash lines inside and the hammer shock with a grey line. The colors represent the driven (blue) and driver (red) gases. The vertical and horizontal direction characterize the time (or angle θ) and the channel length, respectively. The ports are identified by their location as letters "L" used for left and "R" used for right. In the most common four-port reverse flow cycle shown in Fig.2(a), the reactant gas entering the channel (L1) is only exposed to the incidence-reflected shock wave (S_1) heating just prior to the reactant gases being expelled from the channel (L2). Therefore, on-rotor residence time is limited and only exploits a fraction of the full cycle time needed for one full rotation. The different geometries selected for this study seek to address this shortcoming by extending the distance between low-pressure driven inflow (and point of initial shock heating) and the high-pressure outlet port (L4), thus increasing residence time by allowing the processed gas to remain longer in the channel at an elevated temperature. Two new wave cycles (Fig. 2(b) and Fig. 2(c)) will be introduced and analyzed in this work.

The wave cycle (referred to here as Case 1) shown by Fig. 2(b) is composed of a total of 6 ports: the left hand side (LHS

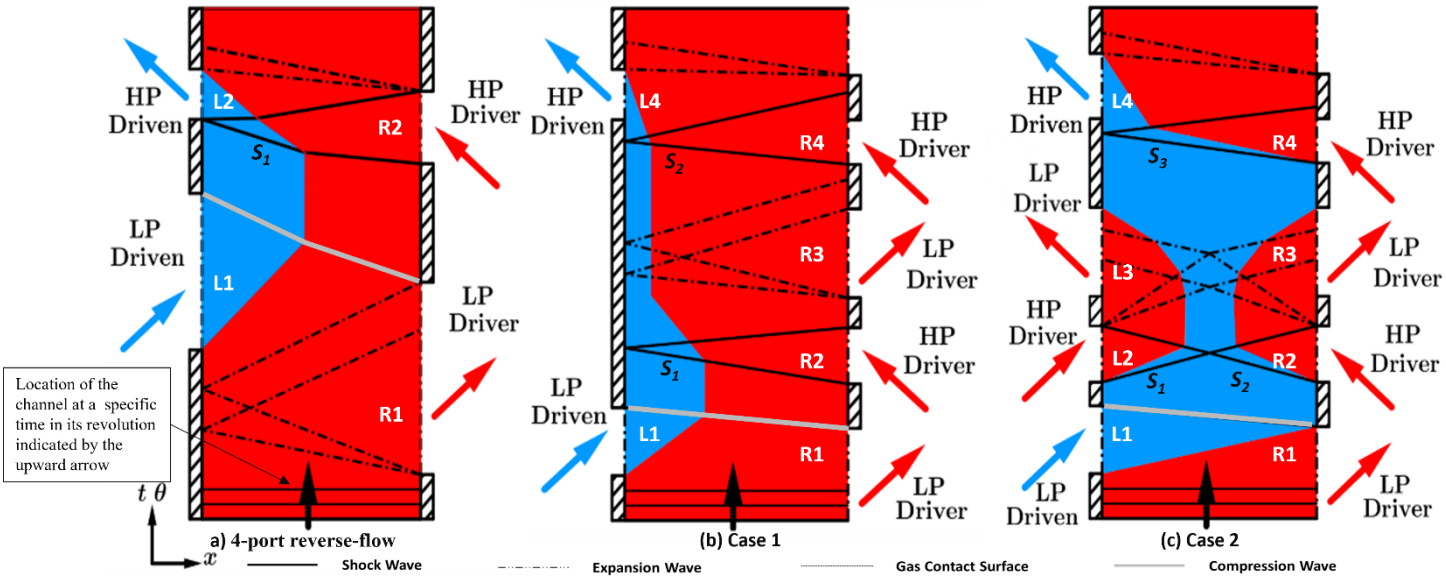

FIGURE 2: REPRESENTING LOCATION OF INLET AND OUTLET GAS AS WELL AS THE PRIMARY AND SECONDARY SHOCK HEATING INVOLVE IN THE CYCLE OPERATION FOR THE THREE WAVE CYCLES, A) 4-PORT REVERSE-FLOW CYCLE B) CASE 1, WITH DOUBLE SHOCK HEATING, C) CASE 2, WITH COLLIDING SHOCK

or driven side) has one inlet port for the low-pressure driven gas (L1) and one outlet port for the high-pressure driven gas (L4). The right hand side (RHS or driver side) has one outlet port for the first low-pressure driver gas (R1) followed by one inlet port for high-pressure driver gas (R2) and this order is repeated for a second driver gas flow (R3 & R4) to give a total of 4 ports. This combination of port timing exposes the reactant gas (L1) to *two pairs* of shock waves - the primary (S_1) and the secondary shocks (S_2), effectively doubling shock heating and providing a significant proportion of rotational time where the driven gases are at high temperature.

Finally, the reformer cycle denoted as Case 2 is shown in Fig. 2(c) and builds on the second configuration of Fig. 2(b). The key difference pertains to the first set of driver ports. The cycle features a symmetric HP driver arrangement leading to a *colliding shock wave system* when two incident shock waves (S_1 and S_2) meet mid-channel. This is aimed to move the peak pressure and temperature (and thus reaction) zone away from the endwall towards the centre of the wave reformer. Further downstream the channel pressure is expanded by two symmetrically arranged LP driver ports. This aims at keeping the methane stream in the centre of the channel and expedite channel scavenging as the expansion takes place on both channels. As a result of this increase in effectiveness, the LP driver lengths can be reduced compared to a one-sided expansion as proposed in the cycles of Fig. 2(a) and 2(b). The preliminary data from modelling this cycle has shown the most promising hydrogen conversion. This cycle requires a total of 8 ports, 4 ports on both sides. The RHS is similar to the previous case but with a difference in the port timing (R1, R2, R3, & R4). However, on the LHS, between the driven gas ports (L1 & L4), two driver ports are added (L2 & L3) that are aligned in term of timing and function to the outlet port for low pressure driver gas (R3) and the inlet port for high pressure driver gas (R2).

2.2 Numerical method

The one-dimensional code (Q1D) used in this paper to compare to the CFD simulation approaches was developed by Tüchler and Copeland and has been presented in previous publication [13, 15]. For this reason, the model will not be described in detail apart from the basic approach. The model follows a channel as it rotates passing the various ports on each end. The aspect ratio of the wave rotor channels is assumed to be sufficiently large for the flow to be treated as one-dimensional. Thus, the code assumes that all quantities are uniform across the channel cross section as functions of time. Q1D uses several non-dimensional data that describe the geometry and key parameters such as port timing, channel width, rotor length, rotational speed.

Even though the Tüchler-Copeland Q1D CFD code [13] offers detailed analysis of fluid dynamics and an excellent understanding of the physics within the channel, the main shortcoming of this model is the difficulty in capturing key flow physics such as the partial opening and mixing as a channel traverses past a port. These detailed fluid dynamic interactions are best simulated by modeling the complete multi channel domain. However, multi channel simulations are much more computationally expensive. Thus, to study the correlation between the design parameters and the characteristics of the flow in the presence of shock waves, a simplified approach is proposed: the quasi-two-dimensional (Q2D) model. This methodology aims to reduce the computational effort while maintaining good agreement between the different modelling approaches in terms of spatial distribution of the pressure gradient for one complete cycle.

2.2.1 Quasi-Two-Dimension Model

The quasi-two-dimensional (Q2D) is using the commercial CFD solver ANSYS Fluent 2020 R20. The model is based on the compressible, and unsteady Navier-Stokes equation coupled with k-ω - SST turbulence closure. In addition, the boundary conditions are implemented through a cell-centered approach with fictitious cells outside of the domain boundaries. Q2D represents the circumferential (tangential) property distribution and interaction within the rotor and stator but by only considering a single cell depth in the radial direction, assumes minimal importance of radial properties. In comparison with a classic 3D, this assumption vastly simplifies the model whilst capturing key flow physics as will be noted later in this paper.

Figure 3 illustrates the fluid domain considered for the simulation by the Q2D approach. It displays two different numerical approaches, a classic 3D numerical model shown in Fig 3(a) and the Q2D approach shown in Fig 3(b), where the fluid domain is represented in solid shade. Fig 3(b), overlays both models. The wireframe represents the initial 3D domain in comparison with the Q2D domain. The blue arrows represent the outlets ports of the domain and the red arrows the inlet ports. The fluid dynamics will be studied along this domain. This represents what we denote as the Q2D model.

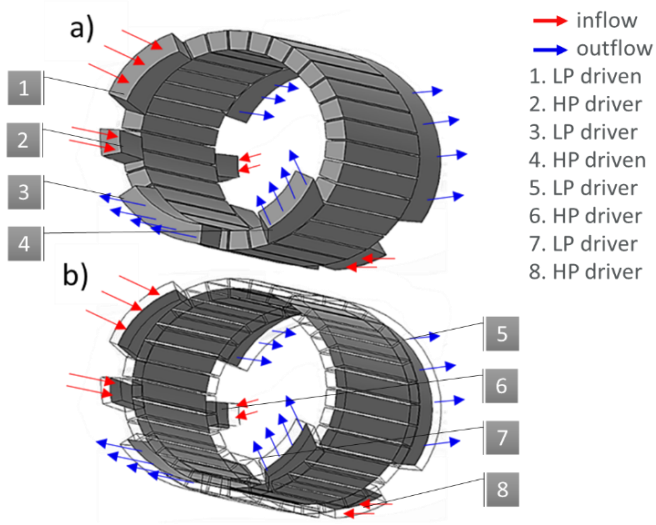

FIGURE 3: SHOWING A COMPARISON BETWEEN TWO DIFFERENT METHODOLOGIES OF SIMULATION, A) 3D MODEL, B) Q-2D MODEL

Nonetheless it is important to consider the impact of the simplification as compared to a full three-dimensional computational domain. Indeed, the radial terms can influence the flow due to the centrifugal effect and friction at shroud and hub. However, this approach aims at reducing the computational effort significantly while retaining major characteristics and flow features. Therefore, the fluid profile was extracted at mid diameter between hub and shroud thereby rendering the domain two-dimensional in the x-plane. As the general flow direction follows the x-axis, this approach ensures reduced deviation of face normal and the flow vector and thus limits the amount of numerical diffusion. The discretization utilizes only one cell in radial direction with each side being modelled as a symmetry surface. Domain discretization was completed using hexahedral elements in Ansys ICEM, different mesh resolutions were performed accordingly to the different configuration. In total the mesh size ranges from approximately 350,000 to 550,000 cells in comparison, the three-dimensional approach requires more than 7,500,000 cells.

2.2.2 Boundary conditions

Due to the unsteady character of the entire domain, transient simulations including an explicit moving mesh for the channels and sliding mesh for each interface between stationary ports and rotating passages were conducted. The governing equations for continuity, momentum, and energy were solved using the unsteady RANS equations with turbulence closure provided through Menter's k-w SST model with enhanced wall treatment. Thus, the flow is assumed to be fully turbulent. The method for hydrogen production is the thermal decomposition of methane. When methane is heated to high temperature, the methane decomposes to carbon and hydrogen. The endothermic thermal decomposition sparks above 973K to separate methane into solid carbon and hydrogen is defined as follow:

$$CH_4 \rightarrow C + 2H_2 \; ; \; \Delta\mathrm{H} \; = \; +75.4 \; \mathrm{KJ/mol} \qquad (1)$$

In order to determine all parameters of the reaction rate, the ensuing system of equations was solved numerically, and the parameters fitted using a least-squares approach to shock tube experimental data conducted by the University of Florida. A thorough description of the fitted modified Arrhenius parameters for the one-step chemistry model used for the decomposition described in a companion paper [14] which will be outlined briefly here. Based on an Arrhenius model of a single step reaction, it shares the description of elementary chemical reactions, leading to a rate coefficient expressed as:

$$K_f = AT^n e^{\frac{-E_a}{RT}}[CH_4]^a \qquad (2)$$

In this equation, A denotes the pre-exponential factor, n is the Arrhenius rate, E_a represents the reaction activation energy, R is the universal gas constant, finally T and a denote the local temperature and the reaction order/rate exponent, respectively. The kinetic parameters for methane pyrolysis used in our RANS simulation are summarized in Table 1.

TABLE 1: FITTED MODIFIED ARRHENIUS PARAMETERS FOR THE ONE-STEP

Pre-exponential factor 1/s]	Arrhenius rate	Activation energy
6.088×10^6	0.1	1.825×10^8

Wave rotor simulations are essentially transient even though near steady-state conditions are present in the ports. Due to the different nature of the cycle, the boundary conditions set at the in- and outflow ports are adapted accordingly to optimize the operating cycle. The high-pressure inlet driver and the low-pressure driven inlet ports are designated as a pressure inlet with a prescribed inlet pressure and inlet temperature. The low-pressure outlet driver and the high-pressure driven outlet ports feature a static backpressure. The conditions remain identical for all the low-pressure outlet driver and high-pressure driver inlet ports. Summary of the boundary conditions are provided in Table 2. The boundary conditions are the results of Q1D analysis, and thus differ slightly for both cases. As the primary purpose of this article is to compare simulation methodology without a thorough review of performance, the boundary conditions have been taken as shown.

TABLE 2: SUMMARY OF BOUNDARY CONDITIONS FOR THE DIFFERENT DESIGNS COMPUTED

	Case 1		Case 2	
	P (bar)	T (K)	P (bar)	T (K)
Driven LP (L1)	2.5	723	2.8	723
Driven HP (L4)	28	1523	45	1454
Driver LP (L3, R1, R3)	1	823	1	900
Driver HP (L2, R2, R4)	40	970	40	950

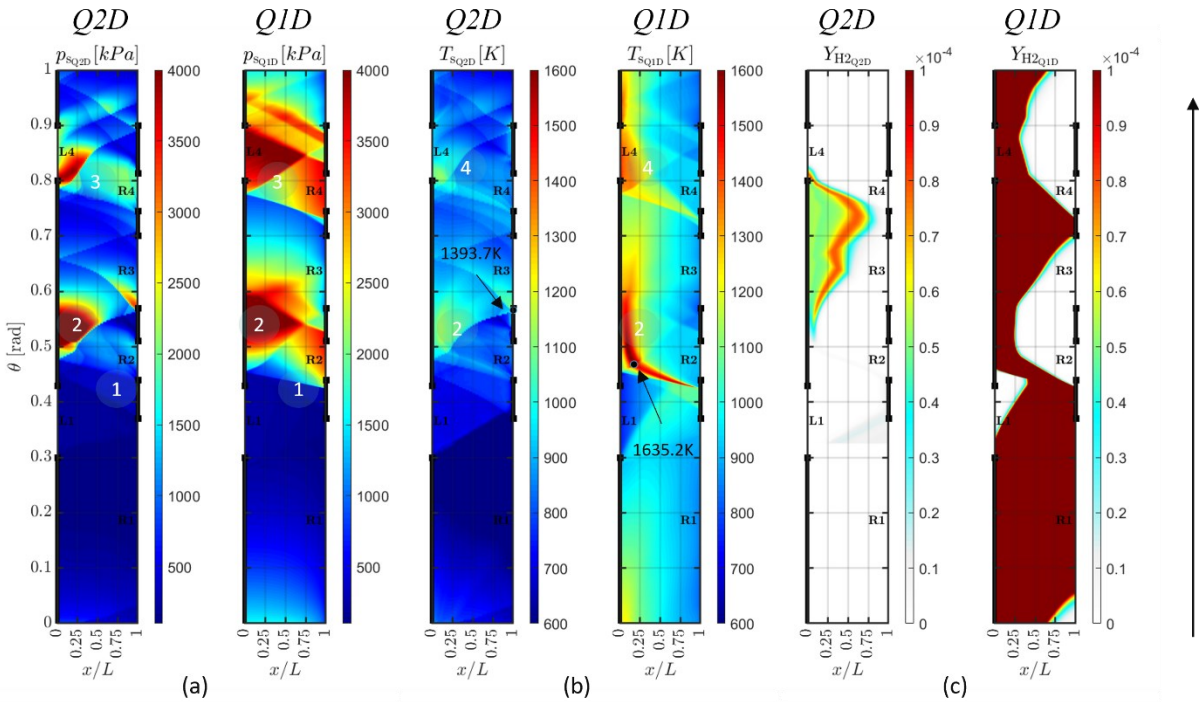

FIGURE 4: COMPARISON BETWEEN Q1D AND Q2D SHOWING (A) STATIC PRESSURE (B) STATIC TEMPERATURE AND (C) HYDROGEN YIELD FOR CASE 1. THE PRESSURE CONTOUR PLOTS OUTLINE A STABLE POSITION OF THE SHOCK AND EXPANSION WAVES WITH RESPECT TO THE PORTS. THE TEMPERATURE FIELD.

3. RESULTS AND DISCUSSION

3.1 Case 1: double shock heating

Figure 4 represents a numerical comparison of Case 1 wave reformer incorporating the wave cycle details discussed previously. Carbon dioxide (CO_2) has been selected as a driver gas for future experimental tests since it is a readily available inert gas that stays relatively safe and stable at high pressure high temperature. Accordingly, pressurized CO_2 flows as driver gas and preheated methane are used as the driven gas. The contour plots in Figure 4 show static pressure, temperature, and hydrogen yield. Number 1-4 denote areas where specific phenomena are examined. Starting from the pressure plot, an area of high pressure is visible after opening the first high pressure inlet port (1) because of the compression by the propagating shock wave. A combination of high-pressure high-temperature region near the LHS is perceptible as the incident shock is reflected (2). The temperature plots indicate high temperature in this region with a peak temperature of 1635K for Q1D and 1393K for Q2D. This temperature increase is approximately double that of the driven inlet port stagnation temperature. After another compression seen at areas (3) and (4), a second region of high-pressure, high temperature is evident. As a consequence of the lower temperature predicted by the Q2D in comparison to the Q1D, the hydrogen yield is not as significant. Numerous factors could have led to this drop, with the most credible resulting from the partial opening/closing effects that create a sudden discharge of pressure within the ports or the channel. As a consequence, the maximum temperature at this location is reduced.

Figure **5** shows partial opening condition as the channels traverse R2 and the resulting high speed jet that results as the channel is first exposed to the high pressure port.

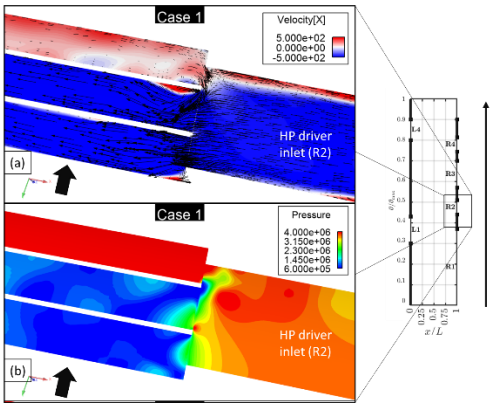

FIGURE 5: REPRESENTS THE FLOW CONTOURS OF VELOCITY (A) AND PRESSURE (B) AT THE SURROUNDING OF THE HP DRIVER INLET (R2). THE CHANNEL DISCHARGES IN THE PORTS.

Overall however, the major flow dynamics are comparable between the two simulation approaches despite lower order of magnitude for most of the key parameters. A small shift in order

of magnitude is visible as well which could be the consequence of the partial opening and mixing loses evident with the Q2D.

Case 2: colliding shocks heating

Figure 6 shows the contour plots of pressure, temperature, and hydrogen yield respectively. Number 1-7 symbolize areas where phenomena are to be discussed. A region of high pressure and temperature is noted in the middle of the channel at the location of the colliding shocks (1). This zone corresponds to the start of hydrogen conversion. The temperature plots indicate high temperature with in this region a peak temperature of 1670K for Q1D and 1450K for Q2D. This is a more than the double the driven inlet port stagnation temperature and significantly greater than Case 1. However, a slight difference between the Q1D and Q2D is visible in Fig.6(d), namely, the highest temperatures are located near the inlet port almost at the entrance (3).

The last HP driver inlet port (R4) triggers the second compression wave which leads to a region of high-pressure, high temperature near the HP driven outlet port (4). From the hydrogen plot, it is evident that the symmetrical shocks trap (6) the hydrogen in the middle of the channel, the hydrogen stays a significant time then exits first on both driver outlet ports and second in the HP driven port (L4). Interestingly the Q2D approach tends to predict hydrogen yield near the hp driver port (L2) (5) due to the high temperature in this area. Some fraction of hydrogen is not completely extracted by the HP driven port and stay within the cycle. The ratio R defined as the port width to channel width is an important parameter denoted. The value R chosen for this configuration is over 4, consequently the port is exposed to 5 channels at the same time. Due to this arrangement of the port, the fluid within the port and channel once exposed to the HP driver inlet port remains highly unstable with flow separation, succession of shocks and flow reversal. These phenomena lead to energy dissipation and a decrease in the thermal energy available for shock compression. It is useful to note that these phenomena are not visible in the Q1D simulation for Case 2 and thus demonstrates the importance of

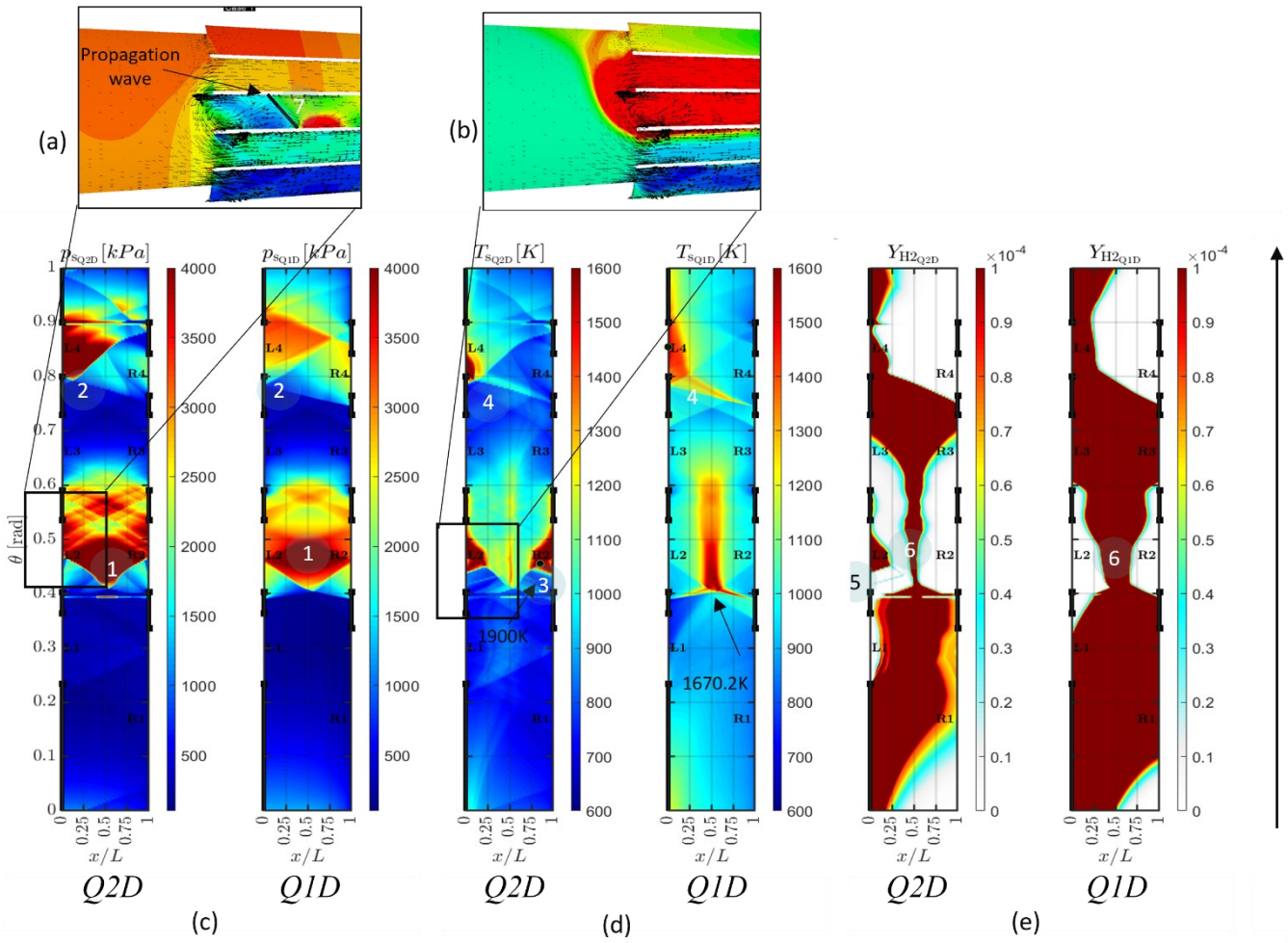

FIGURE 6: COMPARISON BETWEEN Q1D AND Q2D SHOWING (C) PRESSURE AND (D) TEMPERATURE AND (E) HYDROGEN YIELD FOR CASE 2. (A) AND (B) OUTLINE THE GAS DYNAMICS INSIDE THE HIGH-PRESSURE ENTRANCE FOR PRESSURE AND TEMPERATURE, RESPECTIVELY. AT THE INTERFACE PRESSURE DIFFERENTIAL BETWEEN TWO CONSECUTIVE CHANNEL FAVORITES BACKFLOW AND RECIRCULATION FROM CHANNEL-TO-CHANNEL (FROM CHANNEL N TO N-1) AS WELL AS THE TEMPERATURE FIELD

the Q2D approach. Indeed, the ratio for Case 1 was close to the unity (1.25) for the HP driver port R2 and R4 limiting the reflecting shock to discharge the gas in the port. One of the key differences between a single channel wave reformer and the multichannel designs is the interaction that can potentially exist between channels. This is particularly notable in an HP driver port where channel-to-channel circulation is evident in Figure 7. This figure displays the velocity in axial direction with arrows showing flow direction and magnitude at the surroundings of the inlet driver gas on the LHS. Identical trends appear on the RHS HP driver port but only LHS is shown. The port flow is separated in three parts, the lower part, corresponding to the initial opening where the channel rapidly fills at high velocity. This process is visible within the two first channels. The upper segment the channels reverses flow direction and discharges (4,5) into the port. The middle section is composed of separation and backflow. Over time the channel discharges flow in the subsequent channel. The other reason for the reverse flow notable in Fig. 7(a) is that the shock wave arrives back at this port before the port closes This insight can explain one of main sources of difference between the Q2D and Q1D models.

Overall however, the gas dynamics is well represented and consistent within both models. The static pressure plots show a similar position of the shock and expansion waves. Irrespective of the temperature rise differences, the position is consistent and appears in the expected area resulting from the reflected or colliding shocks.

Nonetheless, the strength of the shocks is weaker within the Q2D approach which lead to undesired reduction of maximum temperature since it reduces the pyrolysis potential. Estimated peak temperature difference is approximately 200K compared to the Q1D model which can be viewed as the more optimistic prediction. A small shift in position is visible as well which could be the consequence of the partial opening palpable with the Q2D and thus, the accounting for greater energy dissipation upon shock formation.

The differences identified are the consequence of two major assumption in the Q1D, indeed the model primarily focusses on a single channel and not at the ports in any detail. Consequently, the fluid motion and interactions inside the port are not considered. As we noted for high pressure port, backflow in the region is fully captured in the Q2D simulations. In addition, during a passage partial opening, the Q2D is able to fully model the flow dynamics in this area whereas the 1D simply assumes a binary opening or closing. Thus, the ability to account for how the ports behave is one of the biggest advantages of the Q2D method.

Also, since the Q2D model can forecast the channel-to-channel recirculation and partial opening losses it can be utilized as an asset to increase the first compression shock by tailoring the design to maximize shock strength or minimize energy loss. This will be part of future work using this model, namely to optimize the design.

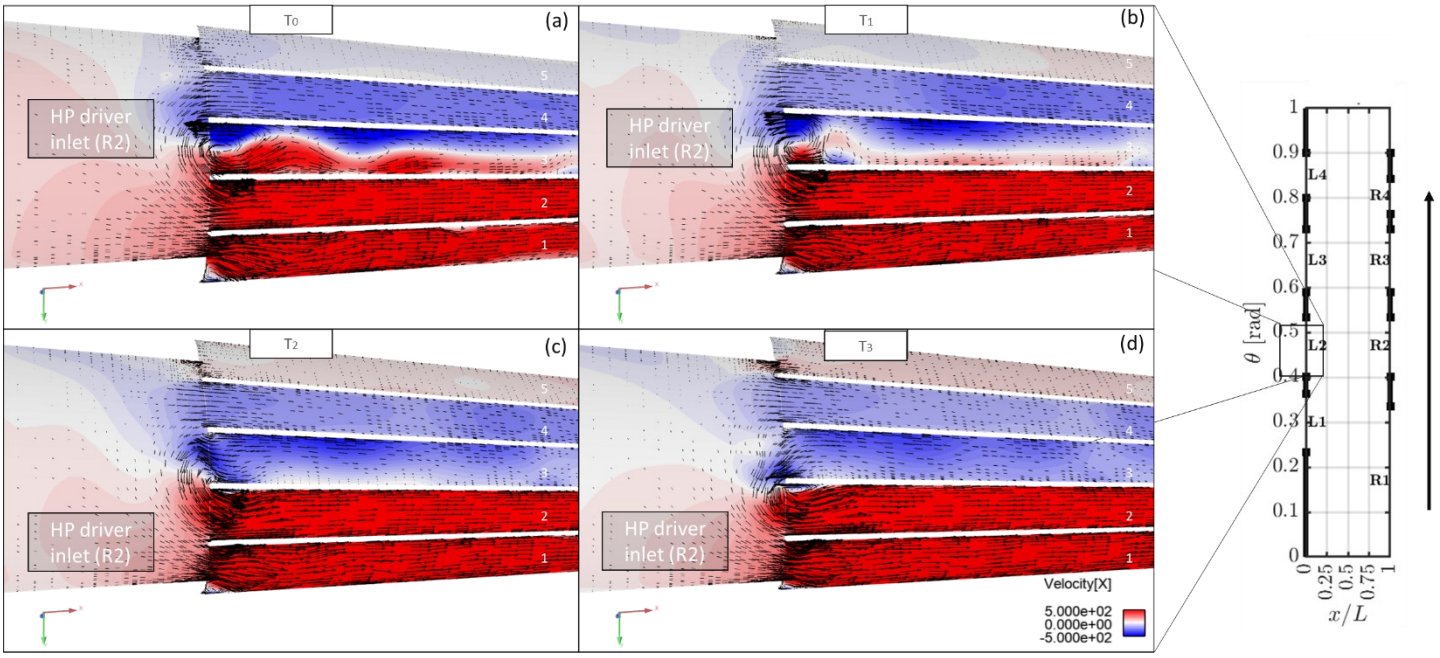

FIGURE 7: SHOWING THE AXIAL VELOCITY AT THE SURROUNDING OF THE HP DRIVER PORTS AT FOUR SEQUENTIAL TIME STEPS T0, T1, T2, T3. RESPECTIVELY (A), (B), (C), (D). THE PORT IS DIVIDED IN THREE SECTIONS, THE LOWER PART (RED COLOR) THE CHANNELS (1&2) ARE FILLED AT HIGH VELOCITY, THE UPPER SEGMENT THE CHANNELS (4,5) DISCHARGE IN THE PORT. IMPORTANT SEPARATION AND BACK FLOW APPEARS IN THE MIDDLE CHANNEL (3) WHICH REFILL THE PREVIOUS CHANNEL.

4. CONCLUSION

In this paper a quasi-two-dimensional model was developed and used to assess the performance of the NWH_2 wave reformer. A comparison study with the Tüchler-Copeland quasi-one-dimensional unsteady model was conducted aimed at identifying key benefit of usage of the Q2D.

To conclude, the main findings of the study can be summarised as follows:

- The simulations show acceptable agreement with the different modelling approaches in terms of spatial distribution of the pressure gradient for one complete cycle.
- Partial opening is a primary performance parameter that needs to be kept for design considerations. It shows time shift in channel filling process. This affects at the same time the scavenges process at the entrance and the wave strength. The Q2D approach provides improved insight to achieve acceptable conditions.
- Losses are amplified at the interface between the stationary ports and the rotating channels.
- Intersection of reflected shocks with inlet ports causes recirculation which is not modelled in the Q1D approach.

In the absence of experimental analysis, the quasi-two-dimensional model permitted to gain further insights and fidelity in the results of the fluid dynamics. Indeed, the Q2D model addresses gaps not covered in the existing model by capturing the fluid dynamics inside the ports the potential flow recirculation inside the port but also interaction at the interface between rotor/stator especially when the opening and closing of port occurs. It led to a better appreciation of the key parameters for future design, and the port timings can be adapted consequently. Furthermore, the relatively low simulation cost is useful to achieve a deeper exploration of the design domain for future work.

The proprietary wave rotor reformer proposed by New Wave Hydrogen Inc. is taking a clear position as an important, sustainable method to produce hydrogen with low energy requirement and in a way where carbon is easily captured. Indeed, the first results shown promising hydrogen conversion ratio that will be studied experimentally in future work.

ACKNOWLEDGEMENT

The authors would like to thank and acknowledge New Wave Hydrogen, Inc. (NWH_2) and co-funding groups including, Emissions Reduction Alberta (ERA), TotalEnergies, the Natural Gas Innovation Fund (NGIF) and its members, and GRTgaz.

REFERENCES

[1] T. da Silva Veras, T. S. Mozer, D. da Costa Rubim Messeder dos Santos, and A. da Silva César, 2017, "Hydrogen: Trends, Production and Characterization of the Main Process Worldwide," *Int. J. Hydrog. Energy*, 42(4), pp. 2018–2033.

[2] J. D. Holladay, J. Hu, D. L. King, and Y. Wang, "An Overview of Hydrogen Production Technologies," *Catal. Today*, 139, pp. 244–260, Jan. 2009. doi: 10.1016/j.cattod.2008.08.039

[3] P. Akbari., C. D. Copeland, S. Tüchler, M. Davidson, and S. V. Mahmoodi-Jezeh, "Shock Wave Heating: A Novel Method for Low-Cost Hydrogen Production" *2021 International Mechanical Engineering Conference*, ASME Paper IMECE2021-69775, Virtual, Online, 2021

[4] T. Ankit, K. Seihra, N. Sen, A. Vatsh, and M. D. Udayakumaran, 2019, "Design and Analysis of Pressure Wave Supercharger," *Int. J Eng. and Techno.* 06(07), p. 5.

[5] D. Hu, R. Li, P. Liu, and J. Zhao, 2016, "The Loss in Charge Process and Effects on Performance of Wave Rotor Refrigerator," *Int. J. Heat Mass Transf.*, 100, pp. 497–507.

[6] P. Akbari, and N. Müller, "Preliminary Design Procedure for Gas Turbine Topping Reverse-Flow Wave Rotors," *Int. Gas Turbine Congress*, p. 8.

[7] P. Akbari, R. Nalim, and N. Müller, "A review of wave rotor technology and its applications", *J. Eng. Gas Turbines Power,* Vol.128 No.4 (2004): pp. 23, doi: 10.1115/1.2204628

[8] D. E. Paxson, "Numerical Simulation of Dynamic Wave Rotor Performance," *J. Propuls. Power*, vol. 12, no. 5, pp. 949–957, Sep. 1996, doi: 10.2514/3.24127.

[9] G. Welch, and R. Chima, 1993, "Two-Dimensional CFD Modeling of Wave Rotor Flow Dynamics," *11th Computational Fluid Dynamics Conference*, American Institute of Aeronautics and Astronautics, Orlando, FL, U.S.A.

[10] S. Chan, and H. Liu, 2017, "Mass-Based Design and Optimization of Wave Rotors for Gas Turbine Engine Enhancement," Shock Waves, 27(2), pp. 313–324.

[11] S. Tüchler, and C. D. Copeland, 2019, "Experimental Results from the Bath μ -Wave Rotor Turbine Performance Tests," *Energy Convers. Manag.,* 189, pp. 33–48.

[12] S. Tüchler, and C. D. Copeland, 2020, "Validation of a Numerical Quasi-One-Dimensional Model for Wave Rotor Turbines with Curved Channels," *J. Eng. Gas Turbines Power,* 142(2).

[13] S. Tüchler, and C. D. Copeland, 2021, "Numerical Optimisation of a Micro-Wave Rotor Turbine Using a Quasi-Two-Dimensional CFD Model and a Hybrid Algorithm," *Shock Waves,* 31(3), pp. 271–300.

[14] S. V. Mahmoodi-Jezeh, S. Tüchler, G. Madiot, P. Akbari, M. Davidson, and C. D. Copeland "Numerical Study of Methane Pyrolysis Inside a Single-Channel Shock Wave Reformer", *ASME Turbo Expo (2022*).